Havel, T. F., Crippen, G. M., & Kuntz, I. D. (1979) *Biopolymers 18*, 73.
Henderson, L. E., Copeland, T. D., Sowder, R. C., Smythers, G. W., & Oroszlan, S. (1981) *J. Biol. Chem. 256*, 8400.
Jentoft, J. E., Smith, L. M., Fu, X., Johnson, M., & Leis, J. (1988) *Proc. Natl. Acad. Sci. U.S.A. 85*, 7094.
Jentoft, J. E., Smith, L. M., & Secnik, J. (1989) *Biophys. J. 55*, 584a.
Karpel, R. L., Henderson, L. E., & Oroszlan, S. (1987) *J. Biol. Chem. 262*, 4961.
Lee, M. S., Gippert, G. P., Soman, K. V., Case, D. A., & Wright, P. E. (1989) *Science 245*, 565.
Macura, S., Ernst, R. R., & Wuthrich, K. (1982) *J. Magn. Reson. 47*, 351.
Marion, D., & Bax, A. (1989) *J. Magn. Reson.* (in press).
Meric, C., & Goff, S. P. (1989) *J. Virol. 63*, 1558.
Parraga, G., Horvath, S. J., Eisen, A., Taylor, W. E., Hood, L., Young, E. T., & Klevit, R. E. (1988) *Science 241*, 1489.
Rance, M., Sorensen, O. W., Bodenhausen, B., Wagner, G., Ernst, R. R., & Wuthrich, K. (1983) *Biochem. Biophys. Res. Commun. 117*, 479.
Redfield, A. G. (1957) *IBM J. Res. Dev. 1*, 19.
Sklenar, V., & Bax, A. (1987) *J. Magn. Reson. 74*, 469.
South, T. L., Kim, B., & Summers, M. F. (1989) *J. Am. Chem. Soc. 111*, 395.
South, T. L., Kim, B., Hare, D. R., & Summers, M. F. (1990) *Biochem. Pharm.* (in press).
Watenpaugh, K. D., Sieker, L. C., & Jensen, L. H. (1980) *J. Mol. Biol. 138*, 615.
Weber, P. L., Morrison, R., & Hare, D. (1988) *J. Mol. Biol. 204*, 483.
Wuthrich, K. (1986) *NMR of Proteins and Nucleic Acids*, Wiley, New York.
Wuthrich, K. (1989) *Science 243*, 45.

# Electrical Potential of Transfer RNAs: Codon–Anticodon Recognition†

Kim A. Sharp,*,‡ Barry Honig,‡ and Stephen C. Harvey§

*Department of Biochemistry and Molecular Biophysics, Columbia University, 630 West 168th Street, New York, New York 10032, and Department of Biochemistry, University of Alabama at Birmingham, Birmingham, Alabama 35294*

*Received July 19, 1989; Revised Manuscript Received August 31, 1989*

ABSTRACT: Calculations of the electrostatic potentials were made around yeast elongator phenylalanine, aspartate tRNAs, and yeast initiator methionine tRNA in aqueous solution at physiological ionic strength. The calculations were carried out with a finite difference algorithm for solving the nonlinear Poisson–Boltzmann equation that incorporates the screening effects of the electrolyte, the exclusion of ions by the molecule, the molecular shape, and the different polarizabilities of the solvent and the tRNA. The initiator tRNA is surrounded by uniformly spaced contours of negative potential. The elongator tRNAs are also surrounded by a similar contour pattern except in the anticodon region where there is a pronounced "hole" in the potential surface. This hole is caused by an invagination of the potential contours, which also results in an increase in the local field strength. The effect of this hole is that the anticodon region in the elongator tRNAs is the least negative, or conversely the most positive, region of the molecule. This hole, which is not found when simple Coulombic potentials are used, is due both to the structure of the elongator tRNA anticodon loops and to the different polarizabilities of the solvent and tRNA. The existence of the potential hole in elongator tRNAs may account in part for their ability to associate with other negatively charged macromolecules, in particular mRNA. Moreover, it suggests that the anticodon loop of elongator tRNAs is the energetically most favorable point of approach of mRNA to tRNA.

Electrostatic interactions play a central role in interactions between biological molecules (Harvey, 1989; Rogers, 1986; Honig et al., 1986). In traditional modeling studies on macromolecules, electrostatic interactions are often described by Coulomb's law (McCammon & Harvey, 1987). However, this approch neglects three important electrostatic factors. First, the polarizability of water is much greater than that of macromolecules, the dielectric constant of the former being about 80 and that of the latter being around 2–4 (Honig et al., 1986; Gilson & Honig, 1986; Nakamura et al., 1988). The effect of solvent screening and presence of a dielectric discontinuity results in the electrostatic forces being dependent not only on the distribution of charge but also on the shape of the macromolecular surface (Warwicker & Watson, 1982; Zauhar & Morgan, 1985; Gilson et al., 1985; Klapper et al., 1986). Second, when the ionic strength of the solvent is nonzero, the electrostatic screening arising from the mobile ions cannot be calculated from Coulomb's law, since the ionic positions are not fixed and can only be described statistically. Third, the ions in the solvent are excluded from the interior of the molecule.

Several recent investigations based on efficient finite difference and finite element numerical solutions to the linear Poisson or Poisson–Boltzmann equation provided more rigorous calculations of electrostatic effects in protein systems (Warwicker & Watson, 1982; Zauhar & Morgan, 1985; Gilson et al., 1985; Klapper et al., 1986). This approach has been used with considerable success in the study of protein structure and enzyme activity (Klapper et al., 1986; Rogers & Sternberg, 1984; Rogers et al., 1985; Warwicker et al., 1985; Gilson &

† This research was supported by grants from the NIH (GM-30518 to B.H.), the NSF (DMB-8706551 to S.C.H.), and the ONR (N00014-86-K0483 to B.H.).
* To whom correspondence should be addressed.
‡ Columbia University.
§ University of Alabama at Birmingham.

0006-2960/90/0429-340$02.50/0 

Honig, 1987; Sternberg et al., 1987). A general conclusion from these studies is that the shape and the low polarizability of a macromolecule can have a large effect on the macromolecular potential.

Nucleic acids present even more of a challenge than proteins, both because they have larger surface-to-volume ratios and because at neutral pH they are highly charged. Until recently it has been difficult to incorporate realistic electrostatic models into calculations on nucleic acid structures. For example, previous molecular mechanics (Harvey & McCammon, 1981; Tung et al., 1984) and molecular dynamics (Harvey et al., 1984, 1985) studies have either omitted or greatly scaled down the phosphate charges because of the problem of adequately treating solvent and ion screening. In a recent study of DNA, we showed that the finite difference method can be used to solve the nonlinear Poisson–Boltzmann equation, which makes it possible to treat highly charged molecules (Jayaram et al., 1989). In this study we investigated the electrostatic potentials around the tRNA molecule.

## Experimental Procedures

The electrostatic potentials in and around yeast phenylalanine ($tRNA^{Phe}$), aspartate ($tRNA^{Asp}$), and initiator methionine ($tRNA_i^{Met}$) transfer RNAs were calculated with the finite difference algorithm to solve the Poisson–Boltzmann equation. The molecule is described in terms of its three-dimensional structure with the location of all charges defined by the coordinates of the appropriate atoms. The coordinates of $tRNA^{Phe}$ were taken from Hingerty et al. (1978), refined by energy minimization, using a standard potential function (Harvey & McCammon, 1981; Tung et al., 1984). The coordinates of $tRNA^{Asp}$ were taken from Westhof et al. (1985) through the Brookhaven data bank. Preliminary coordinates from $tRNA_i^{Met}$ were provided by Professor Paul Sigler. Since in initial studies we were interested in general features of tRNA electrostatics, only the full charges were included, by placing a charge of −0.5 on each nonbridging phosphate oxygen. The positively charged modified bases of $tRNA^{Phe}$, $m^1A58$ and $m^7G46$, are assigned a charge of +1 on the amine nitrogens. Some structures of $tRNA^{Phe}$ include bound counterions (Stout et al., 1978; Dewan et al., 1985), so in one set of our calculations $Mg^{2+}$ ions were included with charges of +2 in the appropriate locations. Bound cation locations are not available for the $tRNA^{Asp}$ and $tRNA_i^{Met}$ structures, so comparisons of potentials between the three molecules are based mainly on the calculations without bound ions. The molecules are assumed to be fully ionized, as would be expected at neutral pH. The net charges are as follows: $tRNA^{Phe}$, −74; $tRNA^{Asp}$, −75; $tRNA_i^{Met}$, −75.

Full details of the method of calculating electrostatic potentials are given elsewhere (Gilson et al., 1988; Jayaram et al., 1989). Briefly, all the charges are treated as being embedded in a low dielectric medium (dielectric of 4), consisting of the volume enclosed by the solvent-accessible surface of the nucleic acid. The surrounding solvent is treated as a continuum of dielectric constant of 80 with an electrolyte behaving according to the nonlinear Poisson–Boltzmann (PB) equation. The Debye screening distance was set at 8 Å, corresponding to the physiological ionic strength of 0.15 M. The nonlinear PB equation is

$$\nabla[\epsilon(x)\nabla\phi(x)] - \kappa'^2(x)\sinh[\phi(x)] + 4\pi\rho(x) = 0 \quad (1)$$

where $\phi$ is the potential expressed in units of $kT/e$, $k$ being Boltzmann's factor, $T$ the absolute temperature, and $e$ the unit proton charge; $\nabla\phi$ is the potential gradient or field, $\epsilon$ is the dielectric constant, and $\rho$ is the fixed charge density. $\epsilon^{1/2}/\kappa'$ is the Debye–Huckel screening length. The quantities $\phi$, $\epsilon$, $\kappa'$, and $\rho$ are all functions of spatial position $x$.

In order to solve eq 1, the nucleic acid and a region of the surrounding solvent are mapped onto a 65 × 65 × 65 grid. The equation is then transformed into $65^3$ simultaneous nonlinear finite difference equations:

$$\phi'_0 = \frac{\sum\epsilon_i\phi_i + 4\pi q_0/d}{\sum\epsilon_i + \kappa'^2d^2[1 + \phi_0^2/3! + \phi_0^4/5! + \ldots + \phi_0^{2n}/(2n+1)!]} \quad (2)$$

where $\phi'_0$ is the new estimate of the potential at a grid point, $\phi_0$ is the previous estimate of the potential at that point, $\phi_i$ ($i$ = 1–6) is the potential at its six neighboring grid points in the positive and negative directions along the $x$, $y$, and $z$ axes, respectively, $\epsilon_i$ is the dielectric constant associated with the midpoints of the six lines joining the point to these neighboring grid points, and $d$ is the grid spacing. The system of simultaneous equations represented by eq 2 can be solved by iterative relaxation as described previously (Gilson et al., 1988), to obtain the potential at all the grid points.

To apply eq 2, each grid point lying in the solvent is assigned a dielectric constant of 80 and a Debye–Huckel parameter representing the required ionic strength ($\kappa^{-1}$ = 8 Å) at an ionic strength of 150 mM). Grid points falling inside the nucleic acid are assigned a Debye–Huckel parameter of zero (mobile ions being excluded), a dielectric constant of 4, and a charge density calculated from the nucleic acid charge distribution. The salt is assumed to be a 1:1 electrolyte, such as NaCl. In the initial calculation the molecule fills about 66% of the grid, giving a scale of about 2 Å per grid. The potential on the grid boundary is approximated with the Debye–Huckel equation (Klapper et al., 1986). In the second part of the calculation, the grid is made 3 times finer and centered on the anticodon loop and the boundary conditions interpolated from the first run, a technique called focusing (Gilson et al., 1988). This permits us to examine the potential around the anticodon with greater resolution.

It should be stressed that although there is some uncertainty as to what the dielectric properties of protein and nucleic acids are, there is general agreement that they are significantly less polarizable than water. In fact, previous studies of electrostatic effects in biomolecules show that neglect of this difference in dielectric behavior, i.e., calculations of potentials based on Coulombic functions, can lead to incorrect models of electrostatic behavior (Gilson & Honig, 1987; Sharp et al., 1987).

To investigate the effect of the difference in polarizability, or dielectric, between the solvent and molecule, calculations were also performed with a molecule dielectric of 80, equal to that of water, but with all other parameters as above. Under these conditions, the molecule still excludes solvent ions since the Debye–Huckel parameter in its interior remains zero, but there is no dielectric boundary.

## Results

Figure 1 shows the phosphate–sugar backbones of the three tRNAs in green, along with the electrostatic potential contours in the range $-0.75kT/e$ (yellow) to $-3.0kT/e$ (blue) around the anticodon stem and loop. The anticodon (bases 34–3l) has been shown in a space-filling representation. It can clearly be seen that for the two elongator tRNAs the potential contours fold in around the anticodon region (Figure 1a,b) and at the $-0.75kT/e$ (outermost) to $-1.0kT/e$ level actually pass below the surface of the molecule. This effectively amounts to a hole in the potential surface at this region. Note also that

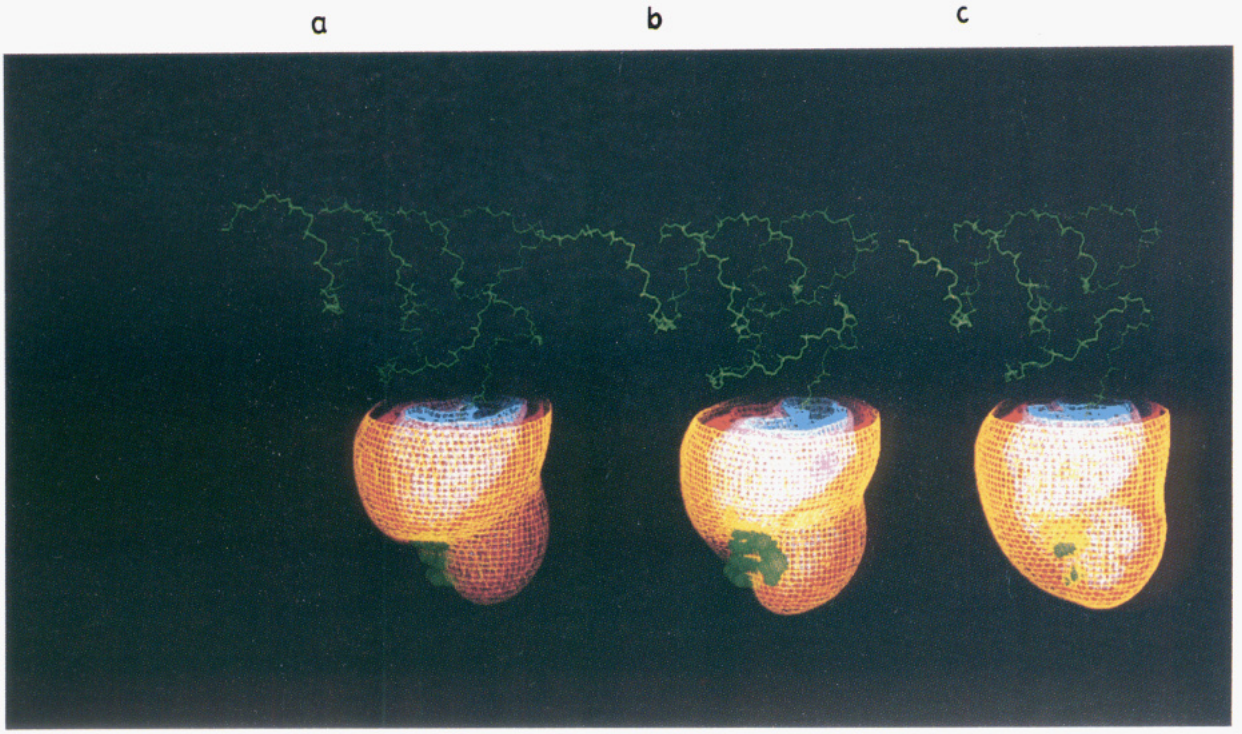


FIGURE 1: Computer graphics representation of the isopotential surfaces around tRNA. Potentials were calculated with a molecule dielectric of 4, a soivent dielectric of 80, and an ionic strength of 0.145 M. A charge of −0.5 was placed on each phosphate oxygen. Contours (in units of $kT/e$) are drawn at −0.75 (yellow), −1.0 (red), −2.0 (magenta), and −3.0 (blue), respectively. Potentials were calculated with the whole molecule, but only portions of the contours around the anticodon loop and stem are displayed. (a) $tRNA^{Phe}$; (b) $tRNA^{Asp}$; (c) $tRNA_i^{Met}$. The phosphate–ribose backbone is shown in green. The anticodon bases 34–36 and the adjacent base 37 are shown in space-filling representation.

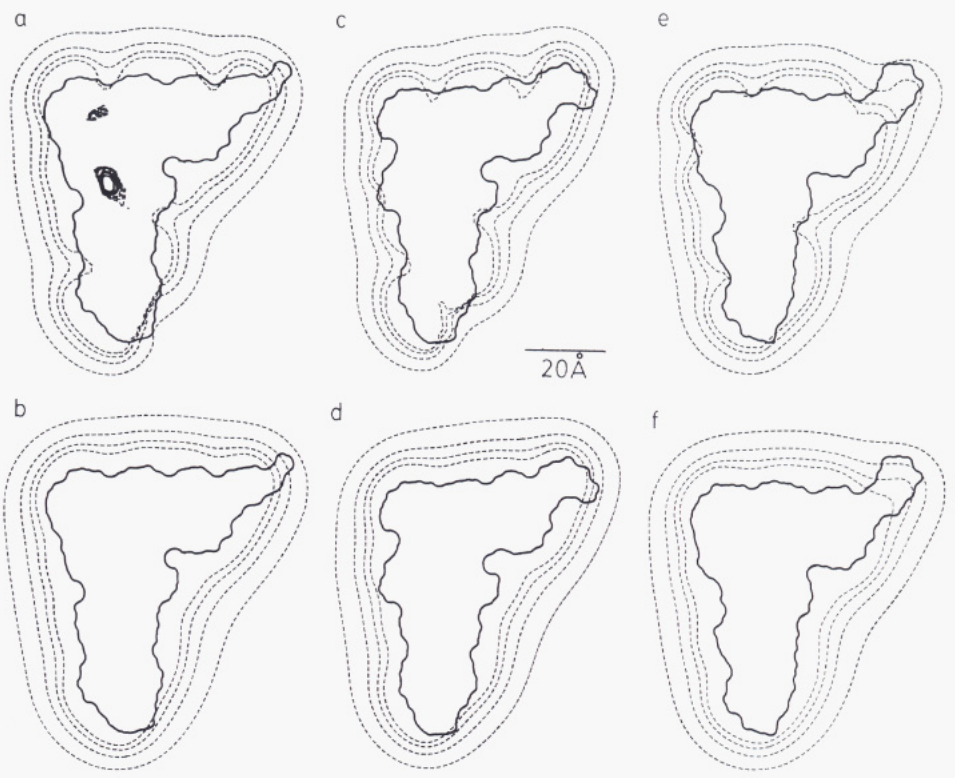


FIGURE 2: Two-dimensional slices through the center of tRNA. The heavy solid line indicates the solvent-accessible surface of the molecules. The amino acid acceptor arm is on the top right, and the anticodon region is on the lower stem of the molecule, facing right. (Panels a and b) $tRNA^{Phe}$; (panels c and d) $tRNA^{Asp}$; (panels e and f) $tRNA_i^{Met}$. (Panels a, c, and e) Conditions as in Figure 1. In Panels b, d, and f the molecule dielectric was set to 80. The dashed lines are isopotential contours at $-0.25kT/e$, $-0.5kT/e$, $-0.75kT/e$, and $-1.0kT/e$ from outermost to innermost. Solid contour lines enclose regions of positive potential.

in this view, the Wye base of $tRNA^{Phe}$, which is believed to play a role in tRNA–mRNA alignment (Saenger, 1984), also protrudes through the potential surface.

Figure 2 shows slices through the solvent-accessible surfaces of the three tRNAs (heavy lines), oriented to show the familiar L-shape, and potential contours at $-0.25kT/e$, $-0.5kT/e$,

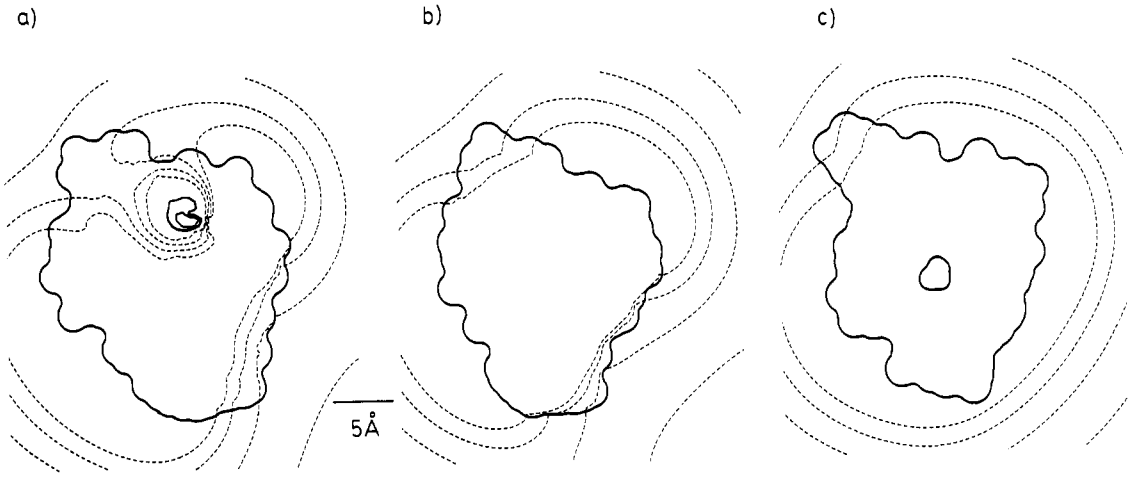


FIGURE 3: Potential contours around part of the anticodon stem and loop. Potentials were calculated as for Figure 1, except only nucleotides 29–41, the anticodon loop, and part of the stem were included. The solvent-accessible surface is shown as a bold line, in the same orientation as Figure 2, i.e., with the anticodon region on the right side. The $tRNA^{Phe}$ potentials (a) also included the effect of the magnesium bound in the anticodon loop region. (b) $tRNA^{Asp}$; (c) $tRNA_i^{Met}$. Contour levels are the same as for Figure 2.

$-0.75kT/e$, and $-1kT/e$ (dashed lines). The anticodon loop is at the bottom of the molecule, with the aminoacyl receptor arm at the top right. Panels a, c, and e, which correspond to the conditions in Figure 1, show that, in regions of the tRNA away from the anticodon, the contours are more uniform, lying around 2–6 Å outside the molecule. The exception is the long 3′ acceptor end which also protrudes through the contour surface. The potential from $tRNA^{Asp}$ is in all respects very similar to that of $tRNA^{Phe}$. The initiator $tRNA_i^{Met}$, by contrast, does not show this necking in of contours in the anticodon region, and the anticodon base lie wholly within the $-1.0kT/e$ contour surface and lower (Figure 2e). The potentials in other regions of the molecule however are very similar to those of $tRNA^{Phe}$ and $tRNA^{Asp}$.

There is another major difference between the potential patterns of initiator tRNA and the two elongator tRNAs. For the two elongator tRNAs the contours crowd closer together in the anticodon region, denoting an increase in the local field strength. By contrast, the $tRNA_i^{Met}$ contours remain evenly spaced, similar to those in the other regions of the molecule.

The effect of the difference in molecular and solvent dielectrics is also shown in Figure 2. The invagination of the contours in the anticodon regions of $tRNA^{Phe}$ and $tRNA^{Asp}$ when the molecule is assigned a dielectric of 4 (Figure 2a,c) disappears when the molecule's dielectric is changed to that of the solvent, 80 (Figure 2b,d). The entire molecule is surrounded by contours of at least $-1kT/e$. For $tRNA_i^{Met}$, which shows no invagination, the effect of the molecule's dielectric on the contour shape is small. The overall pattern for the uniform dielectric cases is similar to that calculated previously from Coulombic potentials derived from charges obtained from a multiple approximation for each ribose, phosphate, and base (Lavery et al., 1980, 1981). The major difference is our use of the water rather than the vacuum dielectric constant, inclusion of the effect of solvent ions through the solution of the Poisson–Boltzmann equation, and exclusion of solvent ions from the molecule interior.

Calculations of the potential for $tRNA^{Phe}$ and $tRNA^{Asp}$ were also carried out with a molecular dielectric of 2, with results very similar to Figure 1. From this and the results in Figure 2 it is clear that the effects are rather insensitive to the exact dielectric used for the molecule, provided it is substantially less than that of water.

Five bound magnesium ions have been located in the crystal structure of $tRNA^{Phe}$ (Stout et al., 1978). One of these is within 10 Å of the anticodon. One set of potential calculations was carried out including the cation charges. The result is to produce localized regions of positive potential around the Mg ions, but these do not extend more than 2–3 Å from the ions and are surrounded by regions of strong negative potential, due to the strongly negative charge of the rest of the tRNA. The negative contours are drawn somewhat closer to the molecule in the region of bases 18–20 since two ions are bound fairly close together, reducing the net charge density, but the pattern of potential in the anticodon region of $tRNA^{Phe}$ remains almost unchanged (Figures 2a and 3a). The positively charged modified bases $m^1A58$ and $m^7G46$ in $tRNA^{Phe}$ are too far away to have a detectable effect on the anticodon potentials.

Calculations were performed on all three RNAs including just the anticodon loop and part of the stem (bases 29–41). The resulting potentials shown in Figure 3 are very similar to those with the whole molecule present. Thus the rest of the molecule has little effect on the pattern of potentials in the anticodon region, due to the effectiveness of solvent and ions in screening the very long-range interactions (the Debye length being about 8 Å at this ionic strength).

## Discussion

Before trying to explain the striking pattern of potentials in the anticodon regions of the two elongator tRNAs $tRNA^{Phe}$ and $tRNA^{Asp}$ and its absent in the initiator $tRNA_i^{Met}$, it is worth making two general observations:

First, although tRNAs have a large negative charge, screening by the water and ions results in potentials close to the surface of the molecules in the range of only a few $kT/e$, which are thus in the range of interest for biological interactions. On the basis of this and previous quantitative successes of the method used here for calculating potentials of proteins (Klapper et al., 1986; Gilson & Honig, 1987; Sternberg et al., 1987), it is likely that the calculations provide a realistic picture of the electrical potential around tRNA.

Second, since the phosphate charges alone give rise to the potential patterns described here, the effects we are seeing are general, in the sense that they are sequence independent. They result only from the conformation of the tRNA, the phosphate charges common to all tRNAs, and the low dielectric of the molecule. Sequence effects would only appear indirectly, insofar as they would result in different conformations. Of course the different charge distributions on the various bases

would modify the potential patterns observed here, perhaps leading to further differences between the different tRNAs. Since the direct electrostatic effect of the bases arises from their permanent dipole potentials, their contribution is very local and is dominated by the monopolar contribution of the phosphates upon moving more than 1–2 Å from the base (Jayaram et al., 1989). The specific electrostatic effects of tRNA bases will be examined in a future study.

Due to the high net negative charge of tRNAs, one might expect the molecule to be uniformly negative, with little variation in the potential pattern due to the phosphates. Indeed, there are only two regions where the negative electrical potential at the molecular surface is less than $1kT/e$: in the anticodon region and near the aminoacyl 3′ end. In the latter case, the van der Waals surface of the tRNA also extends somewhat through the potential surface (top right of Figure 2). However, there is no increase in field here, and the shape of the potential surface in this region is not sensitive to the dielectric used for the tRNA. The protrusion is simply a result of the distance between the 3′ end and the nearest phosphate groups. Although the effective hole in the potential surface is much less pronounced than that in the anticodon region, it could play a role in minimizing electrostatic repulsion between tRNA and the negatively charged aminoacyl adenylate during esterification.

Clearly the most striking observation is the appearance of a hole in the potential surface in the anticodon region of the elongator tRNAs, with a concomitant increase in local field. We first consider the physical origin of this effect and its relationship to the local conformation in the anticodon stem and loop and then discuss whether it may play a role in the biochemical function of tRNA.

There are two factors involved in generating the electrostatic pattern around the elongator tRNA anticodon loops. First, the ribose–phosphate backbone doubles back upon itself at the bottom of the anticodon loop, and the three bases of the anticodon point away from the backbone. Since the phosphate groups, with their large negative charges, are concentrated on one side of the loop (the lefthand side in Figure 2), the bases are relatively far away from all negative charges.

Second, the region of space occupied by the potential hole is separated from the phosphate groups by a low dielectric region formed by the anticodon and flanking bases. This low dielectric "cavity" (low when compared with the surrounding solvent) results in *more* effective screening of the phosphate charges (i.e., an effective dielectric greater than 80). This overscreening effect is best understood within the framework of classical continuum electrostatics [e.g., see Gilson et al. (1985) for this effect in charged spheres]. Similar effects have also been seen in electrostatic calculations on DNA (Jayaram et al., 1989) and in an experimental model of DNA (Troll et al., 1986). Although a full description of this effect is provided only through solutions of the appropriate Poisson or Poisson–Boltzmann equation, a qualitative explanation of this effect may be given as follows: For a charge on the opposite side of a low dielectric region, the low dielectric cavity screens more effectively than the solvent itself by forcing the field lines into the solvent where they must traverse a longer path (Finkel'stein, 1978). Alternatively, one may think of the field from the charge as polarizing the medium around it. At the dielectric boundaries, the difference in polarization is equivalent to the induction of surface charge. On the backside of the dielectric boundary, the surface charge is of opposite sign to the inducing charge. It thus effectively screens the potential arising from the charge.

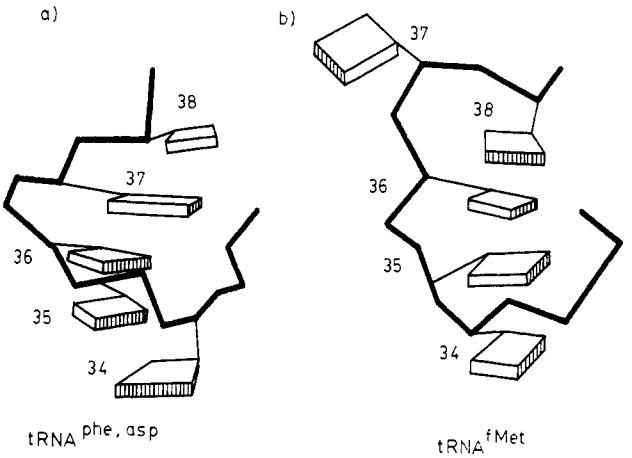


FIGURE 4: Schematic diagram of the base conformations in the anticodon region of elongator tRNAs (a) and initiator tRNA (b). The phosphate–ribose backbone is shown as a bold line; the base-pairing edges of the bases are shaded. Bases 34–36 form the anticodon triplet.

The effect of conformational differences on the pattern of potentials surrounding biomolecules has also been examined in DNA (Matthew & Richards, 1984) and cytochrome *c* (Wendoloski & Matthew, 1989). The former study compared the potentials around A, B, and Z forms of DNA, using a Debye–Huckel type potential function with an effective dielectric constant of 50, while the latter explored different configurations with molecular dynamics using various dielectric functions. Both studies point to the importance of local conformation on potential. However, the elongator anticodon loop conformation alone cannot produce the potential hole, since it disappears if the dielectric boundary is removed (i.e., when a dielectric of 80 is used for both the solvent and the molecule; Figure 2). But neither is the dielectric boundary sufficient to produce this effect, since it is absent in the initiator tRNA. An examination of the structures of the three tRNAs in the region of the anticodon reveals why the effect is absent in the $tRNA_i^{Met}$ structure (Figure 4). In $tRNA^{Phe}$ and $tRNA^{Asp}$, the three anticodon bases, plus the one above (base 37), stack well and are everted, or pointing out from the loop formed by the phosphate backbone. Both the ascending and descending phosphate strands lie behind the bases. In the $tRNA_i^{Met}$ structure base 37 is swung out in an extrahelical conformation. Base 36 of the anticodon is swung up and inward to try to stack with base 38. Bases 34 and 35 follow. This has two effects: The bases are not as everted, lying more between the ascending and descending strands, and there is less low dielectric bulk in the anticodon region. These differences between the elongator tRNAs and the initiator tRNA result in the absence of overscreening around the anticodon of the latter, and thus no potential hole.

It is of interest to consider whether the potential differences observed here both within and between the molecules could play a role in the biological function of tRNA. Considering first the elongator tRNAs, $tRNA^{Asp}$ and $tRNA^{Phe}$, the less negative potentials at the anticodon region would result in different binding energies of a charged molecule or ion to this part of the tRNA. One may think of the $-1kT/e$ contour depicted in Figures 1–3 as a potential barrier of $1kT$ that a single negative charge would have to overcome to approach the tRNA. The hole in the anticodon region means that it would be about $1kT$ easier to bind in this region. Thus the potential pattern could play a role in directing anion binding to the anticodon region or cation binding away from this region. While $1kT$ is not a large difference, for a multivalent

anion the effect would be proportionally larger. For example, when tRNA binds to mRNA, there will be an unfavorable electrostatic repulsion between the two negatively charged molecules. Although this repulsion is probably moderated by the presence of positively charged groups in the ribosome, the orientation of the two RNAs would still be such as to minimize the repulsion. The potential hole at the anticodon could provide access for the mRNA at a minimum cost in electrostatic energy. The regions of the molecule close to the Mg ions are also positive in our potential maps and could also provide attractive sites. However, these regions of potential are very localized, and relatively inaccessible, since the ions tend to be closely "chelated" within the tRNA grooves, and they are still surrounded by regions of negative potential. Previous studies on the effect of electrostatic potentials on association indicate that accessibility is a major factor (Sharp et al., 1987).

The net result of reducing the negative potential is that the anticodon loop has a structure that would minimize the unfavorable electrostatic energy when tRNA binds to mRNA. This may turn out to be a general feature of elongator tRNAs since the two forms examined here have quite different base sequences in this region (ACU-GAA-GAU for $tRNA^{Phe}$ and CUU-GUC-GCG for $tRNA^{Asp}$ respectively for the anticodon and the six flanking bases), yet they both exhibit the potential hole. It will be interesting to examine potential patterns of other tRNAs as their structures become available.

If the structure of the anticodon loop does indeed minimize unfavorable electrostatic interactions with other RNAs, one would also expect that it would play a similar role in tRNA–tRNA interactions. There are two pieces of experimental evidence that support this idea. First, the affinity between complementary RNA triplets is enhanced by 5–6 orders of magnitude when they are built into the anticodon loop of two tRNAs (Eisinger, 1971; Grosjean et al., 1978). Second, anticodon–anticodon interactions are a common feature of tRNA crystal structures. They occur not only in $tRNA^{Asp}$, which has a partly self-complementary anticodon (GUC) (Westhof et al., 1985), but also in the orthorhombic form of $tRNA^{Phe}$, where the anticodon (GAA) has no self-complementarity (Quigley et al., 1974). The monoclinic form of $tRNA^{Phe}$ does not have the head-to-head, tail-to-tail packing pattern of the orthorhombic form, but even in the head-to-tail packing pattern of the monoclinic form, the anticodon loop of one tRNA is in contact with another tRNA (Quigley et al., 1974).

The difference in potential patterns seen between the two elongator tRNAs and the initiator tRNA is also of interest, given the difference in their biochemical function. Initiator tRNA has the ability to bind in the P site of a ribosome in the absence of other ribosomally bound tRNAs and will not bind in the A site. By contrast, elongator tRNAs will only bind to the A site, and then only when the P site is occupied. They subsequently move to the P site during translation (Rich & RajBhandary, 1976). Initiator tRNA also has the ability to form a complex with initiation factor IF2 and GTP. These differences are general properties of the two classes of tRNAs and do not depend on the anticodon sequence. For example, the initiator $tRNA_i^{Met}$ and elongator $tRNA^{E_1}$ which incorporates methionine within proteins have the same anticodon (CAU) yet function differently.

There are two general features of tRNA sequences that distinguish initiators from elongators: First, the end of the acceptor stem of initiators has a non Watson–Crick base pair (usually AU), which may need to be broken during initiation. Second, the anticodon stem of initiators always contains a $(GC)_3$ stack (bases 29–31 and 39–41), while elongators have other, variable sequences (Sigler, 1974). The $(GC)_3$ stack is essential to translation initiation (Seong & RajBhandary, 1987) and also causes differences in the conformation of the anticodon loop, irrespective of the base sequence within the loop (Wrede et al., 1979). The effect of the rest of the tRNA would seem to be smaller, since the anticodon stem and loop fragment of $tRNA_i^{Met}$ binds to the 30S portion of the ribosome in a manner similar to whole $tRNA_i^{Met}$ (Gold, 1988).

From the results obtained here, we suggest that the difference in electrostatic potentials in the anticodon region provide one way in which conformational differences in the stem/loop region could result in differences in binding behavior. The differences in potential we see arise from the phosphate charges only, consistent with the insensitivity to loop sequence.

A note of caution must be sounded here. Although the biochemical evidence clearly indicates differences in anticodon loop conformation, they may not be those revealed by the crystal structures. The different ionic environment within the crystal and the crystal packing forces may result in different structures than those in solution and within the ribosome, particularly since the anticodon regions are often involved in crystal contacts. In addition the pattern of tRNA potentials will be altered upon binding to other molecules, since the latter will displace solvent and solvent ions from around the tRNA. While a quantitative analysis of electrostatic binding energies must await the determination of tRNA–ligand complex structures, it remains true that the less negative the potential, the easier it is to bind anions and the greater the field, the stronger the interaction with dipolar groups.

## Conclusions

A number of conclusions may be drawn from this work. First, rather subtle conformational changes in the anticodon loop structure of tRNA can result in surprisingly large changes in the potential pattern. These are independent of base sequence and result from a combination of conformational and dielectric boundary effects, and they have the effect of reducing the negative potential and increasing the field at the anticodon itself. Second, given these changes in potential, it will be easier to bind negatively charged groups in the anticodon region of elongator tRNAs than elsewhere on the molecule. Finally, in a more general sense, the electrostatic potentials around loops in other RNA molecules will be strongly affected by the local conformation. This may have implications both for the interaction of RNA with other molecules and for the detailed energetics of RNA structures.

One conclusion to be drawn from this work echoes that from our previous studies of the protein Cu,Zn superoxide dismutase (Klapper et al., 1986). There it was suggested that the existence of a large repulsive region of potential away from the active site had little effect on the diffusion of substrate. Rather it was the nature of the active site itself—attractive, neutral, or repulsive and the height of the potential barrier to the active site, if any—that determined the substrate association constant. An analogous argument suggests that the repulsive potential around $tRNA^{Asp}$ and $tRNA^{Phe}$ does not inhibit recognition by mRNA as long as access to the anticodon itself is not inhibited by a large potential barrier. For Cu,Zn superoxide dismutase, this interpretation of the potential maps was subsequently confirmed by calculation of substrate association rates (Sharp et al., 1987). It appears that the structure of elongator tRNAs may have evolved so as to reduce the barrier that might have been expected from such a negatively charged macromolecule, although confirmation of this will have to await experimental

and theoretical determinations of association rates.

ACKNOWLEDGMENTS

We thank Paul Sigler for generously providing us with coordinates for the $tRNA_i^{Met}$ structure and for helpful discussion, F. L. Suddath for information on intermolecular contacts in tRNA crystals, and Larry Gold and D. M. Crothers for helpful conversations.

REFERENCES

Dewan, J., Brown, R. S., & Klug, A. (1985) *Biochemistry 24*, 4785.
Eisinger, J. (1971) *Biochem. Biophys. Res. Commun. 43*, 854.
Finkel'stein, A. V. (1978) *Mol. Biol. (Moscow) 11*, 627.
Gilson, M., & Honig, B. (1986) *Biopolymers 25*, 2097.
Gilson, M., & Honig, B. (1987) *Nature 330*, 84.
Gilson, M., Rashin, A., Fine, R., & Honig, B. (1985) *J. Mol. Biol. 183*, 503.
Gilson, M., Sharp, K., & Honig, B. (1988) *J. Comput. Chem. 9*, 327.
Gold, L. (1988) *Annu. Rev. Biochem. 57*, 199.
Grosjean, H., de Henau, S., & Crothers, D. M. (1978) *Proc. Natl. Acad. Sci. U.S.A. 75*, 610.
Harvey, S. (1989) *Proteins 5*, 78.
Harvey, S. C., & McCammon, J. A. (1981) *Nature 294*, 5838.
Harvey, S. C., Prabhakaran, M., Mao, B., & McCammon, J. A. (1984) *Science 223*, 1189.
Harvey, S. C., Prabhakaran, & McCammon, J. A. (1985) *Biopolymers 24*, 1169.
Hingerty, B., Brown, R. S., & Jack, A. (1978) *J. Mol. Biol. 124*, 523.
Honig, B., Hubbell, W., & Flewelling, R. (1986) *Annu. Rev. Biophys. Biophys. Chem. 15*, 163.
Jayaram, B., Sharp, K., & Honig, B. (1989) *Biopolymers 28*, 975.
Klapper, I., Hagstrom, R., Fine, R., Sharp, K., & Honig, B. (1986) *Proteins: Struct., Funct., Genet. 1*, 47.
Lavery, R., Pullman, A., & Corbin, S. (1981) in *Biomolecular Stereodynamics*, Vol. 1, Adenine Press, New York.
Lavery, R., Pullman, A., & Pullman, B. (1980) *Nucleic Acids Res. 8*, 1061.
Matthew, J. B., & Richards, F. M. (1984) *Biopolymers 23*, 2743.
McCammon, J., & Harvey, S. (1987) in *Dynamics of Proteins and Nucleic Acids*, Chapter 4, Cambridge University Press, Cambridge.
Nakamura, H., Sakamoto, T., & Wada, A. (1988) *Protein Eng. 2*, 177.
Quigley, G. J., Suddath, F. L., McPherson, A., Kim, J. J., Sneden, D., & Rich, A. (1974) *Proc. Natl. Acad. Sci. U.S.A. 71*, 2146.
Rich, A., & RajBhandary, U. (1976) *Annu. Rev. Biochem. 4*, 805.
Rogers, N. (1986) *Prog. Biophys. Mol. Biol. 48*, 37.
Rogers, N. K., & Sternberg, M. (1984) *J. Mol. Biol. 174*, 527.
Rogers, N. K., Moore, G. R., & Sternberg, M. (1985) *J. Mol. Biol. 182*, 613.
Saenger, W. (1984) in *Principles of Nucleic Acid Structure*, Chapter 15, Springer-Verlag, New York.
Seong, B. L., & RajBhandary, U. (1987) *Proc. Natl. Acad. Sci. U.S.A. 84*, 334.
Sharp, K., Fine, R., & Honig, B. (1987) *Science 236*, 1460.
Sigler, P. (1974) *Annu. Rev. Biophys. Bioeng. 4*, 477.
Sternberg, M., Hayes, F., Russell, A., Thomas, P., & Fersht, A. (1987) *Nature 330*, 86.
Stout, C. D., Mizuron, H., Rao, S. T., Swaminathan, P., Rubin, J., Brennan, T., & Sundralingam, M. (1978) *Acta Crystallogr., Sect. B 34*, 1529.
Troll, M., Roitman, D., Conrad, J., & Zimm, B. H. (1986) *Macromolecules 19*, 1186.
Tung, C. S., Harvey, S. C., & McCammon, J. A. (1984) *Biopolymers 23*, 2173.
Warwicker, J., & Watson, H. C. (1982) *J. Mol. Biol. 157*, 671.
Warwicker, J., Ollis, D., Richards, F. M., & Steiz, T. A. (1985) *J. Mol. Biol. 186*, 645.
Wendoloski, J. J., & Matthew, J. B. (1989) *Proteins 5*, 313.
Westhof, E., Dumas, P., & Moras, D. (1985) *J. Mol. Biol. 184*, 119.
Wrede, P., Woo, N. H., & Rich, A. (1979) *Proc. Natl. Acad. Sci. U.S.A. 76*, 3289.
Zauhar, R., & Morgan, R. J. (1985) *J. Mol. Biol. 186*, 815.